PCCP

PAPER

View Article Online
View Journal | View Issue

Cite this: *Phys. Chem. Chem. Phys.*, 2016, **18**, 31924

High-mobility two-dimensional electron gas in $SrGeO_3$- and $BaSnO_3$-based perovskite oxide heterostructures: an *ab initio* study†

Yaqin Wang,[ab] Wu Tang,[a] Jianli Cheng,[b] Safdar Nazir[b] and Kesong Yang*[b]

Received 11th August 2016,
Accepted 27th October 2016

DOI: 10.1039/c6cp05572a

www.rsc.org/pccp

We explored the possibility of producing a high-mobility two-dimensional electron gas (2DEG) in the $LaAlO_3/SrGeO_3$ and $LaGaO_3/BaSnO_3$ heterostructures using first-principles electronic structure calculations. Our results show that the 2DEG occurs at n-type $LaAlO_3/SrGeO_3$ and $LaGaO_3/BaSnO_3$ interfaces. Compared to the prototype $LaAlO_3/SrTiO_3$, $LaAlO_3/SrGeO_3$ and $LaGaO_3/BaSnO_3$ systems yield comparable total interfacial charge carrier density but much lower electron effective mass (nearly half the value of $LaAlO_3/SrTiO_3$), thus resulting in about twice larger electron mobility and enhanced interfacial conductivity. This work demonstrates that $SrGeO_3$ and $BaSnO_3$ can be potential substrate materials to achieve a high-mobility 2DEG in the perovskite-oxide heterostructures.

1 Introduction

The recent development of epitaxial technology has made it possible to achieve high-quality oxide heterostructures (HS) with novel interfacial material properties that are absent in the bulk materials.[1–3] A prominent example is a $LaAlO_3/SrTiO_3$ HS system that consists of two wide band gap insulators $LaAlO_3$ and $SrTiO_3$.[1] This HS system has displayed some unique interfacial properties such as two-dimensional electron gases (2DEGs),[1] superconductivity,[2] and ferromagnetism.[3] These interesting interfacial properties have attracted great attention not only because of its fundamental physics but also because of its promising applications in next-generation nanoelectronics.[1–3]

Although the 2DEG at the $LaAlO_3/SrTiO_3$ interface shows an extremely high charge carrier density,[4,5] its relatively low mobility is still a critical problem and very sensitive to the growth conditions.[6,7] To maximize the function of a perovskite-oxide-based 2DEG for high-performance nanoelectronics, it is necessary to further improve its conductivity with higher charge density and electron mobility. To do this, some approaches such as defect engineering,[8,9] strain engineering,[10–14] and doping engineering[15–18] have been proposed to optimize the interfacial conductive property of perovskite-oxide HS systems. In addition, some experimental efforts have also been made to prepare novel perovskite-oxide-based HS systems such as $NdAlO_3/SrTiO_3$[19] and $LaTiO_3/SrTiO_3$,[20] and to explore their interfacial conductive properties. However, all these perovskite-oxide-based HS systems still use $SrTiO_3$ as the substrate, and the interfacial conductivity is caused by the partially occupied Ti 3d orbitals. It is known that the localized Ti 3d orbital has an intrinsic low-dispersion character, which yields a large electron effective mass and relatively low charge carrier mobility. As a result, even though the charge carrier density could be effectively tuned in the $SrTiO_3$-based HS systems *via* various approaches mentioned above, the charge carrier mobility might not be significantly tuned.

To improve the 2DEG mobility in the perovskite-oxide-based HS systems, one approach is to replace the $SrTiO_3$ with other nonpolar perovskite oxides whose bottom conduction bands are comprised of s or p orbitals. This is because s and p orbitals are less localized than the d orbital, which can potentially lead to larger band dispersion and lower electron effective mass.[21] In terms of this hypothesis, $BaSnO_3$ and $SrGeO_3$ are two potential substrate materials for growing perovskite-oxide HS systems because of their s/p hybridization characters at the bottom of conduction bands.[22,23] Interestingly, several recent experimental studies have provided a solid support for this hypothesis.[24–28] The bulk single crystal of La-doped $BaSnO_3$ has a high room-temperature mobility of 320 $cm^2\ V^{-1}\ s^{-1}$, though the epitaxial films have relatively lower values in the range from 10 to 150 $cm^2\ V^{-1}\ s^{-1}$ in either doped $BaSnO_3$ films or $BaSnO_3$-based HS.[29] Very recently, Bharat Jalan *et al.* have studied the band alignment in epitaxial $BaSnO_3/SrTiO_3$ (001) and $BaSnO_3/LaAlO_3$ (001) HSs using *ex situ* X-ray photoelectron spectroscopy (XPS) and spectroscopic ellipsometry (SE).[29] Correspondingly, a recent computational study revealed that there exists a conduction-band

[a] *State Key Laboratory of Electronic Thin Films and Integrated Devices, University of Electronic Science and Technology of China, Chengdu 610054, P. R. China*
[b] *Department of NanoEngineering, University of California, San Diego, La Jolla, CA 92093-0448, USA. E-mail: kesong@ucsd.edu; Fax: +1-858-534-9553; Tel: +1-858-534-2514*

† Electronic supplementary information (ESI) available. See DOI: 10.1039/c6cp05572a

offset of 1.14 eV at the $BaSnO_3/SrTiO_3$ interface.[30] These experimental and computational studies both suggest that $BaSnO_3$ is an appropriate electron acceptor for $LaAlO_3$ and $SrTiO_3$. Nevertheless, the extremely large lattice mismatch between $BaSnO_3$ and $LaAlO_3$ (about 8%) is pernicious to minimize the defects at the interfacial region or to improve the electron mobility.[25,31] Hence, it is quite necessary to find an alternative perovskite oxide material to match with the $BaSnO_3$ substrate or to find an alternative substrate material with equivalent or higher electron mobility as compared with that of $BaSnO_3$.

In this work, by using first-principles electronic structure calculations, we have modeled $LaAlO_3/SrGeO_3$ and $LaGaO_3/BaSnO_3$ HS systems in which $SrGeO_3$ and $BaSnO_3$ are used as substrate materials, and explored the possibility of producing a high-mobility 2DEG in these two HS systems, respectively. Our results show that these two perovskite-oxide HS systems are able to produce the interfacial metallic states due to the polar catastrophe mechanism, and they keep the comparable total charge carrier density with that of the $LaAlO_3/SrTiO_3$ system. Moreover, by calculating and analyzing electron effective masses, we show that the electron mobility of these two substrate materials is about two times larger than that of $LaAlO_3/SrTiO_3$. These results indicate that, with respect to the model $LaAlO_3/SrTiO_3$ system, an enhanced interfacial electron conductivity is expected in the $LaAlO_3/SrGeO_3$ and $LaGaO_3/BaSnO_3$ HS systems.

2 Computational and structural details

The density functional theory (DFT) calculations were performed using the Vienna *Ab initio* Simulation Package (VASP).[35] The electron–ion interaction was treated by the projector augmented wave (PAW) potential,[36] and the electron exchange–correlation interaction was described by the generalized-gradient approximation (GGA) parameterized by Perdew–Burke–Ernzerhof (PBE).[37] A cutoff energy of 450 eV for the planewave basis set and a Monkhorst–Pack *k*-point mesh of $4 \times 4 \times 1$ were employed. To simulate the epitaxial film growth process in the experiments, the lattice parameters along the *ab*-plane were fixed while those along the *c*-axis and all the ions' positions were fully relaxed until the force tolerance on each atom was smaller than 0.03 eV $Å^{-1}$. All the structural relaxations were carried out using the standard DFT calculations within the GGA-PBE framework. To reproduce the accurate experimental band gap of the parent materials ($BaSnO_3$ and $SrGeO_3$), the Heyd–Scuseria–Ernzerhof (HSE06)[38] hybrid functional was employed in the single-point total energy calculations. The electronic energy convergence was set to 10^{-4} eV, and a Gaussian smearing of 0.08 eV was employed for density of states (DOS) calculations. Although not shown here, the calculated band gaps with varied percent HF exchange contributions show that a 33% HF exchange contribution can yield well the experimental band gaps of 2.7 eV for $SrGeO_3$ and 3.1 eV for $BaSnO_3$, which is exactly the same as the case of SnO_2.[39] Thus, the same HF exchange was used for the following heterostructure calculations.

Table 1 Experimental and calculated structural parameters within the standard DFT-PBE method and band gaps within the DFT-HSE method of cubic $LaAlO_3$, $SrGeO_3$, $LaGaO_3$ and $BaSnO_3$, along with the lattice mismatch (*f*) for the $LaAlO_3/SrGeO_3$ and $LaGaO_3/BaSnO_3$ HS models. "I" ("D") in the bracket stands for the indirect (direct) band gap type

	Experiment			DFT		
Compound	*a* (Å)	*f* (%)	E_g (eV)	*a* (Å)	*f* (%)	E_g (eV)
$LaAlO_3$	3.789[1]	0	5.6(D)[1]	3.811	0	5.36(D)
$SrGeO_3$	3.798[22]	−0.24	2.7(I)[22]	3.859	−1.24	2.68(I)
$LaGaO_3$	3.860[32]	0	4.4(D)[33]	3.939	0	5.26(D)
$BaSnO_3$	4.115[25]	−6.2	3.1(I)[34]	4.186	−5.90	3.13(I)

A superlattice approach was used to model $LaAlO_3/SrGeO_3$ and $LaGaO_3/BaSnO_3$ HS systems that contain symmetrical n-type $(LaO)^+/(SnO_2)^0$ and $(LaO)^+/(GeO_2)^0$ interfaces. To model the HS, 7.5 unit cells of $SrGeO_3$ ($BaSnO_3$) were used as the substrate and 4.5 unit cells of $LaAlO_3$ ($LaGaO_3$) were stacked on the substrate. It is worth mentioning that the superlattice model could exhibit different materials properties from the HS-based slab model in which both the film and the substrate have a surface.[40,41] The difference is mainly caused by the surface effects in the HS-based slab mode in which the film and the substrate both have a surface. For instance, for the well-known $LaAlO_3/SrTiO_3$ system, prior computational studies indicate that only a HS-based slab model can well depict the polarization behavior in the $LaAlO_3$ film though both models can reproduce the interfacial electron reconstruction phenomenon.[40–42]

At room temperature, $BaSnO_3$ crystallizes in a cubic phase,[25] and $LaAlO_3$ and $LaGaO_3$ crystallize in an orthorhombic phase.[43] For $SrGeO_3$, under appropriate conditions such as high pressure and temperature, it can exhibit a cubic phase. For example, Mizoguchi *et al.* prepared the cubic $SrGeO_3$ with a typical perovskite structure upon high-pressure treatment at 1100 °C.[22] Herein, by following the widely used approach,[40,42,44] we built the HS models (1×1 in the *ab*-plane) by treating these non-cubic perovskite oxides as pseudo-cubic structures. In fact, to investigate the possible structural rotation in $LaAlO_3/SrGeO_3$, we also carried out test calculations for a larger HS model by using a $\sqrt{2} \times \sqrt{2}$ supercell in the *ab*-plane. Our calculated energy function *versus* the rotation angle indicates that the structural rotation of the GeO_6 cage is not energetically favorable in this model, see the ESI.† Table 1 lists the experimental and calculated structural parameters and band gaps of $LaAlO_3$, $SrGeO_3$, and $LaGaO_3$ and $BaSnO_3$ in their pseudo-cubic (cubic) phase. The lattice mismatch *f*, defined as $f = (a_f - a_s)/a_s$, for the $LaAlO_3/SrGeO_3$ and $LaGaO_3/BaSnO_3$ HS models is also listed. The negative values of *f* indicate that the film materials experience a tensile strain from the substrate.

3 Results and discussion

3.1 Cleavage energy

To evaluate the strength of interfacial cohesion for the $LaAlO_3/SrGeO_3$ and $LaGaO_3/BaSnO_3$ HS systems, we calculated their cleavage energies utilizing the following formula:[15,45]

$$E_{cleav} = (E^1_{slab} + E^2_{slab} - E_{HS})/2A \quad (1)$$

where E_{HS} is the total energy of the HS system, A is the interfacial area and the factor 2 accounts for two symmetrical interfaces. E^1_{slab} and E^2_{slab} are the total energies of the same supercell containing one material with the other one being replaced by a vacuum. As a proof of concept, we took the HS model $(LaAlO_3)_{4.5}/(SrGeO_3)_{7.5}$ as an example to discuss the procedure of cleavage energy calculations. By following the above notation, E_{HS} refers to the total energy of $(LaAlO_3)_{4.5}/(SrGeO_3)_{7.5}$; E^1_{slab} and E^2_{slab} are the total energies of the $LaAlO_3$ and $SrGeO_3$ slabs, respectively. The $LaAlO_3$ slab was modeled by replacing $SrGeO_3$ with a vacuum in $(LaAlO_3)_{4.5}/(SrGeO_3)_{7.5}$, while the $SrGeO_3$ slab was modeled by replacing $LaAlO_3$ with a vacuum in the HS model. As a result, the vacuum in the two slab models are about 29 and 17 Å, respectively, which is sufficient to avoid artificial interactions between adjacent periodic images. Moreover, the HS model and two slab models share the same size of the supercell, which can cancel out the error to a maximum extent.

The cleavage energy is the energy needed to separate the HS system. That is, a larger cleavage energy indicates a stronger cohesion between the two materials at the interface. The calculated cleavage energies within standard DFT calculations are 0.230 eV $Å^{-2}$ for $LaAlO_3/SrGeO_3$ and 0.241 eV $Å^{-2}$ for $LaGaO_3/BaSnO_3$, respectively, slightly larger than that of the $LaAlO_3/SrTiO_3$ HS system (0.19 eV $Å^{-2}$, ref. 45). This indicates that the n-type $(LaO)^+/(GeO_2)^0$ and $(LaO)^+/(SnO_2)^0$ interfaces are more cohesive than $(LaO)^+/(TiO_2)^0$, and thus the $LaAlO_3/SrGeO_3$ and $LaGaO_3/BaSnO_3$ interfaces are thermodynamically more favorable than the $LaAlO_3/SrTiO_3$ interface.

3.2 Density of states

The calculated total DOS plots of $LaAlO_3/SrGeO_3$ and $LaGaO_3/BaSnO_3$ are shown in Fig. 1. It shows that the Fermi level is pinned to the bottom of conduction bands, indicating typical n-type conductivity. To understand the origin of the metallic electronic states in these two HS systems, we calculated the layer-resolved partial DOSs for $LaGaO_3/BaSnO_3$ and $LaAlO_3/SrGeO_3$ models and are shown in Fig. 2 and 3, respectively. For convenience, here we defined three consecutive SnO_2 (GeO_2) layers, *i.e.*, the 1st, 3rd, and 5th $BaSnO_3$ ($SrGeO_3$) layers as IF-I, IF-III, and IF-V layers, respectively. Our calculations show that the O 2p states in the layers of the substrate materials shift toward high energy with layers moving from the interfacial layer to the deeper layer. The interfacial metallic states are mainly contributed by IF-I, IF-III, and IF-V SnO_2 (GeO_2) layers, and these metallic states are mostly composed of Sn 5s (Ge 4s) and O 2p orbitals, displaying a large energy dispersion within the band gap. The formation of the interfacial metallic states indicates that there exists a polar-catastrophe-driven charge transfer from $LaGaO_3$ to $BaSnO_3$ for the $LaGaO_3/BaSnO_3$ (see Fig. 2) system and from $LaAlO_3$ to $SrGeO_3$ for the $LaAlO_3/SrGeO_3$ (see Fig. 3) system, similar to the case of the $LaAlO_3/SrTiO_3$ system. Interestingly, the

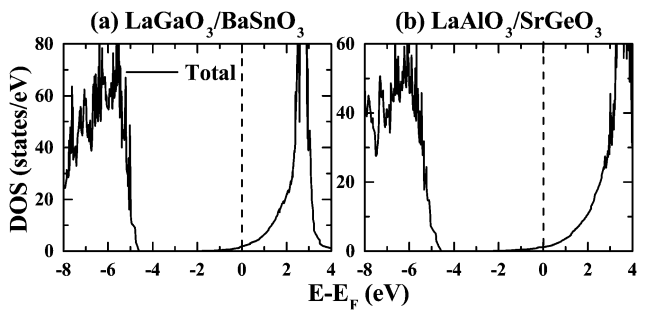

Fig. 1 Calculated total DOSs for (a) $LaGaO_3/BaSnO_3$ and (b) $LaAlO_3/SrGeO_3$ HS systems, respectively. The Fermi level is represented by the vertical dashed line at 0 eV.

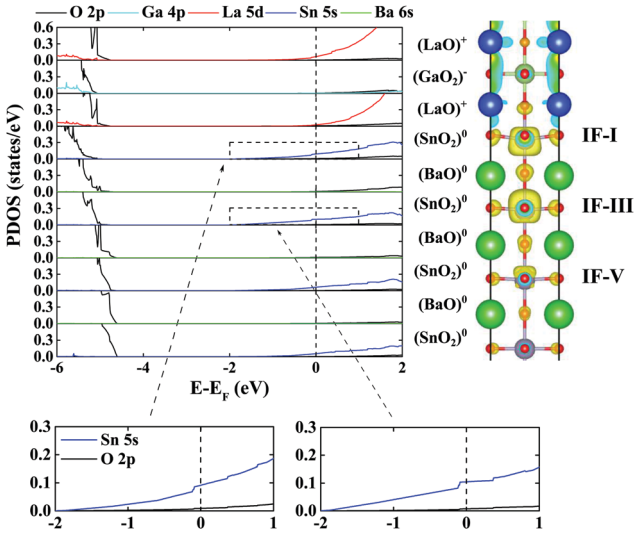

Fig. 2 Calculated layer-resolved partial DOS for the $LaGaO_3/BaSnO_3$ HS system, along with the charge density projected onto bands forming a 2DEG. The isovalue of 6.5×10^{-4} e $Bohr^{-3}$ is used to produce the charge density plots.

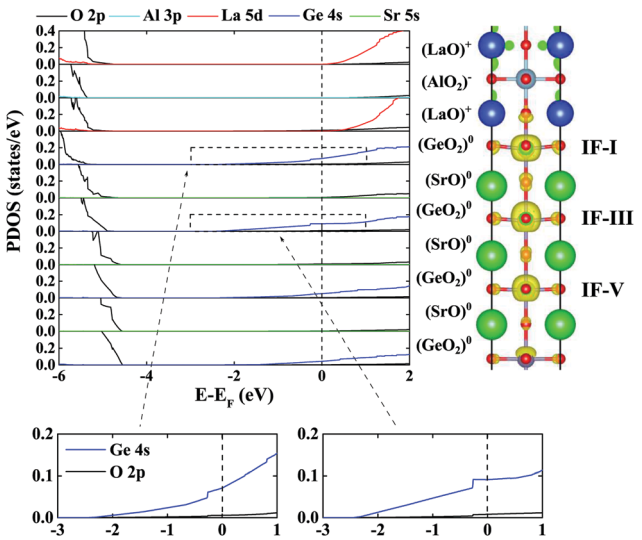

Fig. 3 Calculated layer-resolved partial DOS for the $LaAlO_3/SrGeO_3$ HS system, along with the charge density projected onto bands forming a 2DEG. The isovalue of 1.7×10^{-3} e $Bohr^{-3}$ is used to produce the charge density plots.

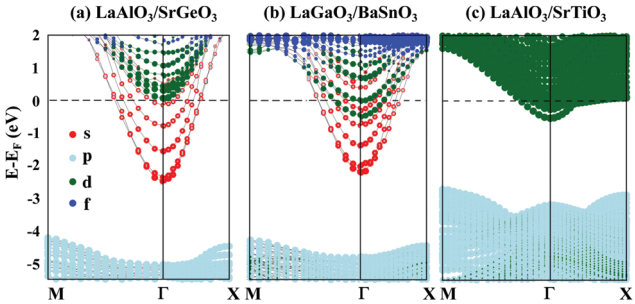

Fig. 4 Calculated electronic band structures of (a) $LaAlO_3/SrGeO_3$ and (b) $LaGaO_3/BaSnO_3$ within the DFT-HSE approach. For comparison, the electronic band structure of $LaAlO_3/SrTiO_3$ produced from spin-restricted DFT calculations is shown in (c). The horizontal dash line indicates that the Fermi level is at zero.

largest charge densities for $LaGaO_3/BaSnO_3$ ($LaAlO_3/SrGeO_3$) HS systems occur in the IF-III SnO_2 (GeO_2) layer. This is mainly because the SnO_6 (GeO_6) octahedra in the IF-I layer have a larger structural distortion than that in the IF-III layer. The structural distortion produces a dipole moment towards the deep layers, leading to more charge transfer to the IF-III layer. This fact is different from the case of the $LaAlO_3/SrTiO_3$ HS system, in which the 2DEG mainly resides in the IF-I TiO_2 layer.[11] In addition, in the $LaGaO_3/BaSnO_3$ system (see Fig. 2 and 4b), few electrons released from the interfacial $(LaO)^+$ layer are also transferred to La 5d orbitals in its adjacent $(LaO)^+$ layer, forming partially occupied La 5d states. As discussed below, the partially occupied La 5d states also increase the electron effective mass of the $LaGaO_3/BaSnO_3$ system. In contrast, interestingly, the $LaAlO_3/SrGeO_3$ system (see Fig. 3 and 4a) does not show a similar phenomenon. This implies that La 5d orbitals have much weaker ability to capture electrons compared to Ge 4s orbitals and Sn 5s orbitals either, but to a lesser extent for the later.[21] Therefore, La 5d orbitals are partially occupied in the $LaGaO_3/BaSnO_3$ system.

3.3 Band structures and effective masses

Next, we calculated the electronic band structures for the $LaAlO_3/SrGeO_3$ and $LaGaO_3/BaSnO_3$ HS systems along the path M–Γ–X of the interfacial Brillouin zone, along with that of the prototype $LaAlO_3/SrTiO_3$ HS system for a direct comparison (see Fig. 4c). As shown in the band structures, some electronic states reside below the Fermi level in all the three HS systems, indicating an n-type conductivity in the systems. For the $LaAlO_3/SrTiO_3$ HS system (non-spin-polarized calculation), the light band d_{xy} around Γ is parabolic and the heavy band extends along the Γ–X direction. In contrast, in the case of $LaAlO_3/SrGeO_3$ and $LaGaO_3/BaSnO_3$ HS systems (see Fig. 4a and b), the hybridization between Ge 4s (Sn 5s) states and O 2p states leads to more delocalized conduction bands near the Fermi level than that of the $LaAlO_3/SrTiO_3$ system, and thus a smaller electron effective mass is expected.

To quantitatively verify this inference, we then calculated the electron effective mass, m^*/m_e, for the minimum conduction bands along the Γ–X and Γ–M directions, in which m_e is the free electron rest mass. The effective mass m^* was calculated using the parabolic approximation using the formula:[46]

$$\frac{1}{m^*} = \frac{1}{\hbar^2}\frac{\partial^2 E_{CB}}{\partial k^2} \quad (2)$$

where $\hbar$ is the reduced Planck constant, E_{CB} the energy of the minimum conduction band, and k the wave vector corresponding to the conduction bands. The calculated effective masses along the Γ–X and Γ–M directions for the three HS systems are listed in Table 2. For the $LaAlO_3/SrTiO_3$ HS system, the calculated relative effective mass m^*/m_e is 0.49 along the Γ–X direction, which is well consistent with previous calculation.[47] For the $LaAlO_3/SrGeO_3$ and $LaGaO_3/BaSnO_3$ HS systems, the calculated m^*/m_e along the Γ–X direction are 0.20 and 0.24, respectively, which are nearly half of the value for the $LaAlO_3/SrTiO_3$ HS system. This is because the minimum conduction bands of the $LaAlO_3/SrGeO_3$ ($LaGaO_3/BaSnO_3$) HS systems are comprised of Ge 4s (Sn 5s) and O 2p orbitals, while those of the $LaAlO_3/SrTiO_3$ HS system is comprised of Ti 3d orbitals, and the former are more delocalized than the latter. Since the electron mobility is inversely proportional to the electron effective mass, the $LaAlO_3/SrGeO_3$ and $LaGaO_3/BaSnO_3$ HS systems are expected to have a higher 2DEG mobility than the $LaAlO_3/SrTiO_3$. It is worth pointing out that the calculated m^*/m_e for the $LaAlO_3/SrTiO_3$ and $LaGaO_3/BaSnO_3$ HS systems is in good agreement with that of the bulk $SrTiO_3$ (0.46[48]) and $BaSnO_3$ (0.20–0.22[49,50]), indicating that the interfacial 2DEG of the HS oxide systems inherits the bulk materials properties from their parent constituent materials.

Table 2 Calculated electron effective masses (in units of free electron mass) along the Γ–X and Γ–M directions from the superlattice model using spin-restricted DFT calculations

Systems	m^*/m_e	
	Γ–X	Γ–M
$LaAlO_3/SrGeO_3$	0.20	0.22
$LaGaO_3/BaSnO_3$	0.24	0.25
$LaAlO_3/SrTiO_3$	0.49	0.51

3.4 Charge carrier density, mobility and conductivity

Besides the charge carrier mobility, the interfacial charge carrier density is also an important factor in determining the interfacial conductivity of the 2DEG. To have a quantitative comparison of the interfacial charge carrier density among the $LaAlO_3/SrGeO_3$, $LaGaO_3/BaSnO_3$, and $LaAlO_3/SrTiO_3$ HS systems, we calculated the total and layer charge carrier densities by integrating their total and layer-resolved partial DOSs for the conducting gap states below the Fermi level, see Fig. 5a. Our calculations show that these three HS systems nearly show a comparable total charge density of about 3.0–3.5 $\times$ 10^{14} cm^{-2}, which corresponds to a charge transfer of $0.5e^-$ from the polar $LaAlO_3$ ($LaGaO_3$) to the nonpolar $SrTiO_3$ ($SrGeO_3$ and $BaSnO_3$) substrate. This indicates that the polar catastrophe at the $(AO)^+/(BO_2)^0$ interface can drive about $0.5e^-$ charge transfer, which is independent of the choice of the substrate. It is worth

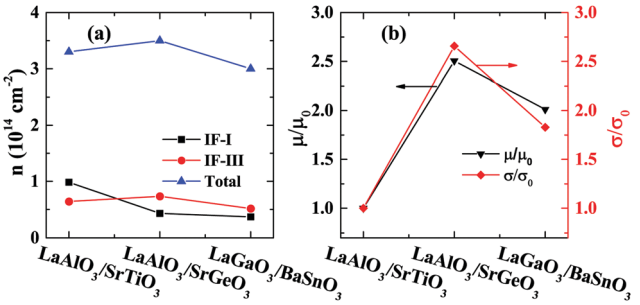

Fig. 5 (a) Calculated total and IF-I and IF-III layer charge carrier densities and (b) normalized electron mobility (μ/μ_o) and conductivity (σ/σ_o) of $LaAlO_3/SrGeO_3$ and $LaGaO_3/BaSnO_3$ with respect to $LaAlO_3/SrTiO_3$.

mentioning that the present calculations are based on the superlattice model, which leads to a higher charge carrier density than that of the HS-based slab model.[41]

To have a direct comparison of the interfacial conductivity among these three HS systems, we calculated the normalized charge carrier mobility (μ/μ_0) and conductivity (σ/σ_0) with respect to those of the $LaAlO_3/SrTiO_3$ system, see Fig. 5b. μ_0 and σ_0 refer to the charge carrier mobility and conductivity of the $LaAlO_3/SrTiO_3$ HS system, respectively. The following two equations were used:[51] $\mu = e\langle\tau\rangle/m^*$ and $\sigma = ne\mu$, in which e, $\langle\tau\rangle$, m^*, n, μ, and σ are the elementary charge, average scattering time (also called "relaxation time"),[51,52] electron effective mass, charge carrier density, electron mobility, and electrical conductivity, respectively. The scattering time τ is determined by all the scattering events such as impurity scattering, electron–phonon scattering, and electron–electron scattering, and the inverse of τ can be expressed as the sum of rates associated with different scattering mechanisms according to Matthiessen's rule.[53] It has been extremely challenging to calculate the scattering time τ due to the complicated scattering mechanism. One common and simplified approach is to treat τ as a constant under the constant scattering (relaxation) time approximation,[54,55] which has been validated in prior studies.[46,56,57] In this work, by assuming that $\langle\tau\rangle$ is a constant, our calculations show that the electron mobility and the electrical conductivity of $LaAlO_3/SrGeO_3$ and $LaGaO_3/BaSnO_3$ HS systems are nearly 2.5 and 2.0 times larger than those of the $LaAlO_3/SrTiO_3$ HS system, respectively. This indicates that using $BaSnO_3$ and $SrGeO_3$ as the host substrates one can effectively improve the charge carrier mobility and conductivity of the 2DEG.

4 Conclusions

In conclusion, first-principles electronic structure calculations are employed to explore the possibility of producing a high-quality 2DEG in the $LaAlO_3/SrGeO_3$ and $LaGaO_3/BaSnO_3$ HS systems. Our results reveal that these two HS systems can form interfacial metallic states consisting of less localized Ge 4s and Sn 5s orbitals, respectively, which leads to smaller electron effective mass and higher charge carrier mobility compared to the well-known $LaAlO_3/SrTiO_3$ HS model. This work shows a feasible route to enhance the 2DEG mobility and interfacial conductivity using novel substrate materials such as $SrGeO_3$ and $BaSnO_3$.

Acknowledgements

This work was supported by the National Science Foundation under the award number ACI-1550404 and a Department of Defense National Security Science and Engineering Faculty Fellowship (under the ONR contract number N000141510030). This work used the Extreme Science and Engineering Discovery Environment (XSEDE), which is supported by a National Science Foundation grant number OCI-1053575. Y. W. is grateful for the visiting graduate student fellowship from the University of Electronic Science and Technology of China.

References

1 A. Ohtomo and H. Y. Hwang, *Nature*, 2004, **427**, 423–426.
2 N. Reyren, S. Thiel, A. D. Caviglia, L. F. Kourkoutis, G. Hammer, C. Richter, C. W. Schneider, T. Kopp, A. S. Rüetschi, D. Jaccard, M. Gabay, D. A. Muller, J. M. Triscone and J. Mannhart, *Science*, 2007, **317**, 1196–1199.
3 A. Brinkman, M. Huijben, M. van Zalk, J. Huijben, U. Zeitler, J. C. Maan, W. G. van der Wiel, G. Rijnders, D. H. A. Blank and H. Hilgenkamp, *Nat. Mater.*, 2007, **6**, 493–496.
4 S. Thiel, G. Hammerl, A. Schmehl, C. W. Schneider and J. Mannhart, *Science*, 2006, **313**, 1942–1945.
5 W. Siemons, G. Koster, H. Yamamoto, W. A. Harrison, G. Lucovsky, T. H. Geballe, D. H. A. Blank and M. R. Beasley, *Phys. Rev. Lett.*, 2007, **98**, 196802.
6 T. Fix, F. Schoofs, J. L. MacManus-Driscoll and M. G. Blamire, *Phys. Rev. Lett.*, 2009, **103**, 166802.
7 T. Hernandez, C. W. Bark, D. A. Felker, C. B. Eom and M. S. Rzchowski, *Phys. Rev. B: Condens. Matter Mater. Phys.*, 2012, **85**, 161407.
8 Z. Liu, C. Li, W. Lü, X. Huang, Z. Huang, S. Zeng, X. Qiu, L. Huang, A. Annadi, J. Chen, J. Coey, T. Venkatesan and Ariando, *Phys. Rev. X*, 2013, **3**, 021010.
9 L. Weston, X. Cui, S. Ringer and C. Stampfl, *Phys. Rev. Lett.*, 2014, **113**, 186401.
10 B. Kalisky, E. M. Spanton, H. Noad, J. R. Kirtley, K. C. Nowack, C. Bell, H. K. Sato, M. Hosoda, Y. Xie, Y. Hikita, C. Woltmann, G. Pfanzelt, R. Jany, C. Richter, H. Y. Hwang, J. Mannhart and K. A. Moler, *Nat. Mater.*, 2013, **12**, 1091–1095.
11 S. Nazir, M. Behtash and K. Yang, *Appl. Phys. Lett.*, 2014, **105**, 141602.
12 S. Nazir and K. Yang, *ACS Appl. Mater. Interfaces*, 2014, **6**, 22351–22358.
13 S. Nazir, M. Behtash and K. Yang, *RSC Adv.*, 2015, **5**, 15682–15689.
14 Z. Huang, Z. Q. Liu, M. Yang, S. W. Zeng, A. Annadi, W. M. Lü, X. L. Tan, P. F. Chen, L. Sun, X. Renshaw Wang, Y. L. Zhao, C. J. Li, J. Zhou, K. Han, W. B. Wu, Y. P. Feng,

J. M. D. Coey, T. Venkatesan and Ariando, *Phys. Rev. B: Condens. Matter Mater. Phys.*, 2014, **90**, 125156.
15 S. Nazir, J. Cheng, M. Behtash, J. Luo and K. Yang, *ACS Appl. Mater. Interfaces*, 2015, **7**, 14294–14302.
16 S. Nazir, M. Behtash, J. Cheng, J. Luo and K. Yang, *Phys. Chem. Chem. Phys.*, 2016, **18**, 2379–2388.
17 T. Yajima, Y. Hikita, M. Minohara, C. Bell, J. A. Mundy, L. F. Kourkoutis, D. A. Muller, H. Kumigashira, M. Oshima and H. Y. Hwang, *Nat. Commun.*, 2015, **6**, 6759.
18 S. Nazir, C. Berna and K. Yang, *ACS Appl. Mater. Interfaces*, 2015, **7**, 5305–5311.
19 X. Xiang, L. Qiao, H. Xiao, F. Gao, X. Zu, S. Li and W. Zhou, *Sci. Rep.*, 2014, **4**, 5477.
20 J. Biscaras, S. Hurand, C. Feuillet-Palma, A. Rastogi, R. Budhani, N. Reyren, E. Lesne, J. Lesueur and N. Bergeal, *Sci. Rep.*, 2014, **4**, 6788.
21 L. Bjaalie, B. Himmetoglu, L. Weston, A. Janotti and C. G. V. de Walle, *New J. Phys.*, 2014, **16**, 025005.
22 H. Mizoguchi, T. Kamiya, S. Matsuishi and H. Hosono, *Nat. Commun.*, 2011, **2**, 470.
23 S. Ismail-Beigi, F. J. Walker, S.-W. Cheong, K. M. Rabe and C. H. Ahn, *APL Mater.*, 2015, **3**, 062510.
24 H. J. Kim, T. H. Kim, W.-J. Lee, Y. Chai, J. W. Kim, Y. J. Jwa, S. Chung, S. J. Kim, E. Sohn and S. M. Lee, *et al.*, *Thermochim. Acta*, 2014, **585**, 16–20.
25 P. V. Wadekar, J. Alaria, M. OSullivan, N. L. O. Flack, T. D. Manning, L. J. Phillips, K. Durose, O. Lozano, S. Lucas, J. B. Claridge and M. J. Rosseinsky, *Appl. Phys. Lett.*, 2014, **105**, 052104.
26 K. Ganguly, P. Ambwani, P. Xu, J. S. Jeong, K. A. Mkhoyan, C. Leighton and B. Jalan, *Appl. Mater.*, 2015, **3**, 062509.
27 Z. Lebens-Higgins, D. Scanlon, H. Paik, S. Sallis, Y. Nie, M. Uchida, N. Quackenbush, M. Wahila, G. Sterbinsky and D. A. Arena, *et al.*, *Phys. Rev. Lett.*, 2016, **116**, 027602.
28 S. Raghavan, T. Schumann, H. Kim, J. Y. Zhang, T. A. Cain and S. Stemmer, *Appl. Mater.*, 2016, **4**, 016106.
29 S. A. Chambers, T. C. Kaspar, A. Prakash, G. Haugstad and B. Jalan, *Appl. Phys. Lett.*, 2016, **108**, 152104.
30 K. Krishnaswamy, L. Bjaalie, B. Himmetoglu, A. Janotti, L. Gordon and C. G. Van de Walle, *Appl. Phys. Lett.*, 2016, **108**, 083501.
31 H. Mun, U. Kim, H. Min Kim, C. Park, T. Hoon Kim, H. Joon Kim, K. Hoon Kim and K. Char, *Appl. Phys. Lett.*, 2013, **102**, 252105.
32 P. Perna, D. Maccariello, M. Radovic, U. Scotti di Uccio, I. Pallecchi, M. Codda, D. Marré, C. Cantoni, J. Gazquez, M. Varela, S. J. Pennycook and F. M. Granozio, *Appl. Phys. Lett.*, 2010, **97**, 152111.
33 K. Ogisu, A. Ishikawa, Y. Shimodaira, T. Takata, H. Kobayashi and K. Domen, *J. Phys. Chem. C*, 2008, **112**, 11978–11984.
34 W. Zhang, J. Tang and J. Ye, *J. Mater. Res.*, 2007, **22**, 1859–1871.
35 G. Kresse and J. Furthmüller, *Phys. Rev. B: Condens. Matter Mater. Phys.*, 1996, **54**, 11169–11186.
36 P. E. Blöchl, *Phys. Rev. B: Condens. Matter Mater. Phys.*, 1994, **50**, 17953–17979.
37 J. P. Perdew, K. Burke and M. Ernzerhof, *Phys. Rev. Lett.*, 1996, **77**, 3865–3868.
38 J. Heyd, G. E. Scuseria and M. Ernzerhof, *J. Chem. Phys.*, 2003, **118**, 8207–8215.
39 M. Behtash, P. H. Joo, S. Nazir and K. Yang, *J. Appl. Phys.*, 2015, **117**, 175101.
40 W.-J. Son, E. Cho, B. Lee, J. Lee and S. Han, *Phys. Rev. B: Condens. Matter Mater. Phys.*, 2009, **79**, 245411.
41 M. Behtash, S. Nazir, Y. Wang and K. Yang, *Phys. Chem. Chem. Phys.*, 2016, **18**, 6831–6838.
42 R. Pentcheva and W. E. Pickett, *Phys. Rev. Lett.*, 2009, **102**, 107602.
43 D. Lybye, F. W. Poulsen and M. Mogensen, *Solid State Ionics*, 2000, **128**, 91–103.
44 Z. Zhong, P. X. Xu and P. J. Kelly, *Phys. Rev. B: Condens. Matter Mater. Phys.*, 2010, **82**, 165127.
45 S. Nazir, M. Behtash and K. Yang, *J. Appl. Phys.*, 2015, **117**, 115305.
46 G. Hautier, A. Miglio, D. Waroquiers, G.-M. Rignanese and X. Gonze, *Chem. Mater.*, 2014, **26**, 5447–5458.
47 N. Bristowe, E. Artacho and P. Littlewood, *Phys. Rev. B: Condens. Matter Mater. Phys.*, 2009, **80**, 045425.
48 A. Janotti, D. Steiauf and C. Van de Walle, *Phys. Rev. B: Condens. Matter Mater. Phys.*, 2011, **84**, 201304.
49 H.-R. Liu, J.-H. Yang, H. Xiang, X. Gong and S.-H. Wei, *Appl. Phys. Lett.*, 2013, **102**, 112109.
50 S. Dabaghmanesh, R. Saniz, M. Amini, D. Lamoen and B. Partoens, *J. Phys.: Condens. Matter*, 2013, **25**, 415503.
51 Y. Peter and M. Cardona, *Fundamentals of semiconductors: physics and materials properties*, Springer Science & Business Media, 2010.
52 P. B. Allen, W. E. Pickett and H. Krakauer, *Phys. Rev. B: Condens. Matter Mater. Phys.*, 1988, **37**, 7482–7490.
53 M. C. Karamargin, C. A. Reynolds, F. P. Lipschultz and P. G. Klemens, *Phys. Rev. B: Condens. Matter Mater. Phys.*, 1972, **6**, 3624–3633.
54 T. J. Scheidemantel, C. Ambrosch-Draxl, T. Thonhauser, J. V. Badding and J. O. Sofo, *Phys. Rev. B: Condens. Matter Mater. Phys.*, 2003, **68**, 125210.
55 J. Yang, L. Xi, W. Qiu, L. Wu, X. Shi, L. Chen, J. Yang, W. Zhang, C. Uher and D. J. Singh, *npj Comput. Mater.*, 2016, **2**, 15015.
56 G. K. H. Madsen, *J. Am. Chem. Soc.*, 2006, **128**, 12140–12146.
57 W. Chen, J.-H. Pohls, G. Hautier, D. Broberg, S. Bajaj, U. Aydemir, Z. M. Gibbs, H. Zhu, M. Asta, G. J. Snyder, B. Meredig, M. A. White, K. Persson and A. Jain, *J. Mater. Chem. C*, 2016, **4**, 4414–4426.